Composite electrolytes based on electrospun PVDF and ionic plastic crystal matrices for Na-metal battery applications

IOP Publishing J. Phys. Mater. 4 (2021) 034003 https://doi.org/10.1088/2515-7639/abeed2

Journal of Physics: Materials

OPEN ACCESS

RECEIVED
29 December 2020

REVISED
2 March 2021

ACCEPTED FOR PUBLICATION
15 March 2021

PUBLISHED
14 April 2021

PAPER

Composite electrolytes based on electrospun PVDF and ionic plastic crystal matrices for Na-metal battery applications

Faezeh Makhlooghiazad[1,2,*], Frederick Nti[1], Ju Sun[1], Tiago Correia Mendes[1], Sneha Subhas Malunavar[1], Jennifer M Pringle[1,2] and Maria Forsyth[1,2]

[1] Institute for Frontier Materials (IFM), Deakin University, Burwood, Victoria 3125, Australia
[2] ARC Centre of Excellence for Electromaterials Science, Deakin University, Deakin University, Burwood, Victoria 3125, Australia
[*] Author to whom any correspondence should be addressed.

E-mail: f.makhlooghiazad@deakin.edu.au

Keywords: solid-state electrolyte, sodium battery, organic ionic plastic crystals

Supplementary material for this article is available online

Abstract

Sodium ion batteries are widely considered to be a feasible, cost-effective, and sustainable energy storage alternative to Lithium, especially for large-scale energy storage applications. Next generation, safer electrolytes based on ionic liquid (IL) and organic ionic plastic crystals (OIPCs) have been demonstrated as electrochemically stable systems which show superior performance in both Li and Na applications. In particular, phosphonium-based systems outperform most studied nitrogen-based ILs and OIPCs. In this study triisobutyl(methyl)phosphonium bis(fluorosulfonyl)imide ($[P_{1i444}][FSI]$) OIPC mixed with 20 mol% of NaFSI or NaTFSI were combined with an electrospun polyvinylidene fluoride (PVDF) support to create self-standing electrolyte membranes, and their thermal phase behaviour and ionic conductivity were investigated and compared with the bulk electrolytes. The ability of the solid-state composite electrolytes to support the cycling of sodium metal with good efficiency and without breakdown were examined in sodium metal symmetrical coin cells. The sodium transference number was determined to be 0.21. The electrochemical performance of $Na/Na_3V_2(PO_4)_3$ cells incorporating the composite electrolytes, including good cycling stability and rate capability, is also reported. Interestingly, the mixed anion systems appear to outperform the composite electrolyte containing only FSI anions, which may relate to electrolyte interactions with the PVDF fibres.

1. Introduction

Society is fast approaching a transition towards a renewable energy economy supported by a robust energy storage network. However, the accelerating global uptake of EVs and grid-scale battery storage raises serious concerns over the sustainability and reserves of raw materials that would be needed to meet these demands. In particular, unsustainable mining of global reserves of lithium, cobalt, nickel, and graphite could potentially become constrained if the current trends and predictions are met, leading to shortages and potential conflict [1]. New battery chemistries are therefore required and can be targeted for suitability towards certain segments of the economy, e.g. mobility, grid-scale, portable electronics [2]. Sodium ion chemistries are an exciting new area of battery development owing to the fact that their performance is now approaching that of current Lithium ion technologies, but with the advantage of being composed of earth-abundant raw materials [3, 4]. Despite the larger ion size and sometimes slower ion dynamics in the electrolyte, Na ion batteries (NIBs) can surprisingly outperform the high rate capability of the best Li ion chemistries [5]. These properties of NIBs make them an excellent candidate to supersede Li ion chemistries for many applications where the higher energy density provided by Lithium is not necessary [6, 7]. This includes large-scale grid applications, mobility applications (lower driving range affordable EVs, electric bikes, buses etc.), telecommunication backup and many others; wherever raw materials cost and sustainability of enormous production volumes is critical, and high power applications where high rate performance is needed.

In all battery technologies, the electrolyte plays a critical role in performance and safety. Current commercial technologies are based on flammable organic solvents with serious safety problems [8, 9]. To improve the safety and reliability of batteries, all-solid-state batteries using solid electrolytes are being studied as next-generation systems [10–14]. The main characteristics of solid electrolytes needed for practical battery applications are high ion conductivity, good mechanical flexibility, and high thermal and electrochemical stability. Organic ionic plastic crystals (OIPCs) are a group of solid-state electrolytes that have shown favourable properties in terms of safety and performance in Na and Li devices [12, 15–18]. These materials typically have long-range ordered crystalline structures with rotational/orientational motions of ions that give them interesting properties such as plastic deformation under external pressure. These properties can significantly improve the interfacial contact with the electrode materials and thus enhance battery performance. OIPCs also have high thermal and electrochemical stability [19–21]. Although there has been many scientific reports regarding OIPC application in Li batteries [22–26], very few reports have been published on sodium batteries [27, 28].

Forsyth *et al* reported solid-state electrolytes based on the 1-ethyl-1-methylpyrrolidinium bis(trifluoromethylsulfonyl)imide ([C_2mpyr][TFSI]) OIPC and a wide range of NaTFSI concentrations. They found that these binary mixtures have a high temperature eutectic transition (63 °C) with high ionic conductivity of 10^{-4} S cm^{-1} for 40 mol% NaTFSI at 60 °C, which is in the solid state [12]. Interestingly, Hagiwara *et al* showed that replacing TFSI anion with FSI in the same cation OIPC and sodium salt results in the mixtures that are liquid in a wide temperature range. They also reported stable cycling performance of 60 mol% NaFSI in [C_2mpyr][TFSI] at 90 °C in Na metal cell using a $Na_3V_2(PO_4)_3$ (NVP/C) cathode material [29]. It was shown that phosphonium based OIPCs and ionic liquid (IL) provide benefits including higher ionic conductivity and wider electrochemical stability compared to their nitrogen-based cation analogues [30, 31].

We report a comprehensive phase diagram of mixtures of P_{111i4}TFSI with NaTFSI, and the relationship of the phase behaviour of each composition with their local structure and dynamics of sodium ions was investigated. It was shown that for highly concentrated NaTFSI/OIPC mixtures, the materials are quasi-solid above 45 °C due to the peritectic transition. Stable stripping and plating of sodium metal in a sodium symmetrical cell incorporating high concentration of NaTFSI (75 mol% NaTFSI) was also demonstrated for the first time, showing the applicability of phosphonium-based OIPC electrolytes in sodium devices [15]. A binary system containing an OIPC with a bulkier phosphonium cation ($[P_{1i444}]^+$) and a smaller anion (FSI) with different concentrations of NaFSI resulted in enhanced ionic conductivity and superior electrochemical properties in terms of stable and reversible stripping and plating of Na metal in a Na symmetrical cell [28]. Sodium metal batteries based on these electrolytes with NVP/C and $NaFePO_4$ cathode materials were also developed and showed good performance at 60 °C, at which point the capacity of organic solvent electrolytes decays fast, usually failing after just a few cycles [27].

However, in some cases the mixture of OIPCs with Li or Na salts results in soft solid, quasi-solid or liquid electrolytes that can be readily deformed under low pressure and having no mechanical strength. Therefore, an advance OIPC electrolyte with enhanced mechanical properties is greatly desirable for their practical use in high performance devices. One strategy for enhancing mechanical integrity is to combine an OIPC or IL electrolyte with a polymer to create a polymer composite electrolyte. Different polymer materials have been added to IL/soft OIPC materials mixed with Li and Na salts in order to improve their mechanical properties and attain self-standing membranes for Li and Na devices [32–35]. Wang *et al* showed the addition of electrospun polyvinylidene fluoride (PVDF) nanofiber into a composite polymer electrolyte based on poly(diallyldimethylammonium) bis(trifluoromethanesulfonyl)amide (PDADMA TFSI), N–propyl–N–methylpyrrolidinium bis(fluorosulfonyl)imide ([C_3mpyr][FSI]) IL and high concentration LiFSI salt improves their mechanical properties. These ion gel electrolytes possess high a transference number of 0.53 and showed promising performance with high areal capacity of 1.1 mAh cm^{-2} in a Li metal full cell with high-voltage $LiNiMnCoO_2$ and $LiNi_{0.8}Co_{0.15}Al_{0.05}O_2$ cathode materials [36]. Free-standing composite electrolytes composed of PVDF nanofibers and 10 and 50 mol% LiFSI in [C_2mpyr][FSI] OIPC resulted in desirable mechanical properties and electrochemical performance [22, 23]. A composite electrolyte including PVDF nano-particles/LiFSI-[C_2mpyr][FSI] OIPC in a ratio of 60/40 wt% showed around one order of magnitude increase in ionic conductivity and a high Li ion transference number. High capacity (119 mA g^{-1} at 2 C) with long-term stability was achieved in a Li/$LiFePO_4$ cell with this composite electrolyte [37]. Anastro *et al* reported an ion gel electrolyte based on polyDADMA-TFSI, [C_3mpyr][FSI] IL and NaFSI salt. It was shown that the addition of alumina nanoparticles into the membrane increase the mechanical properties whilst slightly decreasing the ionic conductivity. A full cell based on a sodium metal anode and a $NaFePO_4$ cathode material with good capacity retention of 110 mAh g^{-1} at C/20 and high coulombic efficiency (>97%) was demonstrated [11].

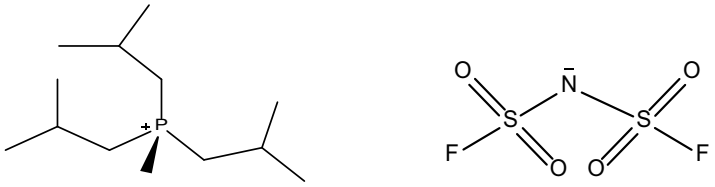

Figure 1. Chemical structure of triisobutyl(methyl)phosphonium bis(fluorosulfonyl)imide [P_{1i444}] [FSI].

It has also been shown that there is a potential advantage in using mixed anions in terms of achieving a higher ionic conductivity and lower viscosity and improved cell cycling [38–40]. For example, a significant enhancement in physico-chemical properties, including lower viscosity, higher thermal stability and improved ionic conductivity, was reported upon mixing the IL 1-ethyl-3-methylimidazolium ([emim]) TFSI with LiFSI. Improved battery performance in terms of higher capacity (152 mAh g^{-1} at 0.05 C at 75 °C) and stability was also observed in Na/$NaFePO_4$ cells incorporating (butylmethylpyrrolidinium–bis(trifluoromethanesulfonyl)imide) BMP−TFSI-based ILs with $NaBF_4$ [41]. Superior interfacial behaviour due to the formation of a homogeneous, conductive SEI layer was also reported using a mixture of N–methyl–N–propylpyrrolidinium dicyanamide IL with a saturated concentration of NaFSI, resulting in long cycle life with low polarization potential [39].

In this work we develop safer solid-state composite electrolytes based on [P_{1i444}][FSI]/NaFSI and [P_{1i444}][FSI]/NaTFSI combined with electrospun PVDF fibers. The phase behaviour, ionic conductivity and Na ion transference number of the composite electrolytes were examined and the compatibility of the electrolytes with sodium metal was studied. The composite electrolytes delivered high capacity with high coulombic efficiency in Na/$Na_3V_2(PO_4)_3$ cells at 50 °C, demonstrating the promise of these new phosphonium cation-based ionic membrane materials.

2. Material and methods

2.1. Electrolyte preparation

Triisobutyl(methyl)phosphonium bis(fluorosulfonyl)imide [P_{1i444}][FSI] (figure 1) was synthesized as described in [42]. Sodium bis(fluorosulfonyl)amide (NaFSI) (99.99%) and sodium bis(trifluoromethanesulfonyl)amide (NaTFSI) (99.99%) were purchased from Solvionic and used without further purification. Mixtures of 20 mol% of NaFSI or NaTFSI in [P_{1i444}][FSI] were prepared inside an argon-atmosphere glove box. Homogeneous solutions were achieved for both these mixtures. All samples were stored in sealed vials inside an argon atmosphere glove box. The chemical structure of [P_{1i444}][FSI] is presented in figure 1.

Electrospun PVDF fibrous membranes were made by dissolving 11 wt% PVDF (KF850, from Kureha Chemicals, Japan) in 1:1 volume ratio of acetone and N,N–dimethylformamide. The solution was sonicated for 2 h and stirred at 60 °C overnight. The resulting uniform solution was loaded in a 10 ml syringe, connected to a needle (Terumo, 20 G × 1.5′). The syringe was positioned 20 cm away from the collecting rotating drum covered with aluminium foil, the voltage applied was 17.5 kV and the solution was fed at a rate of 4 ml h^{-1} for 2 h. The obtained fibres were 4 mm thick. PVDF membranes with a diameter of 14.5 mm were punched and dried in vacuum at 50 °C for 24 h.

The free-standing electrolyte composites were composed of 15 wt% of electrospun PVDF nanofibres and 85 wt% of OIPC-salt binary solutions. This was done by impregnating the OIPC salt-solutions into the electrospun PVDF membranes to form a flexible membrane as shown in figure S1 (available online at stacks.iop.org/JPMATER/4/034003/mmedia).

2.2. Thermal analysis

The thermal behaviour of the samples was studied by differential scanning calorimetry on a Mettler Toledo DSC1 instrument, which runs on a STAReV6.10 software. 10–12 mg of samples were sealed in Al pans inside a glovebox under an Ar atmosphere. Two scans were recorded for each sample with 10 °C min^{-1}. The samples were held at an isothermal temperature of −120 °C for 10 min before heating to 120 °C.

2.3. Galvanic cycling measurements

All symmetric cells fabricated in CR2032 coin cells purchased from Hoshen Corporation, Japan inside an argon-filled glove box. The membranes were sandwiched between two sodium discs (Sigma Aldrich, 99.9%

purity) of 6 mm diameter with 0.5 mm spacer and 1.4 mm spring to ensure good contact. The cells were rested inside an oven at 50 °C for 24 h prior to cycling. All cells were cycled employing chronopotentiometry with 0.2 mA cm^{-2} applied current density for 1 h stripping and 1 h plating of Na for 100 cycles. Before long term cycling, the rate capability of 20 mol% NaFSI in $[P_{1i444}][FSI]$ and 20 mol% NaTFSI in $[P_{1i444}][FSI]$ was studied by applying different current densities (0.05 up to 0.5 mA cm^{-2}, five cycles at each current density). A multi-channel Potentiostat VMP3/Z (Bio-Logic) driven by EC-lab software version 11.27 was used for the sodium symmetric cell measurements.

2.4. Transference number measurement

Sodium symmetrical cells were constructed in the same process as described above forthe galvanic cycling measurements and used to measure Na^+ transference number at 50 °C based on the potentiostatic polarisation method described by Evans, Bruce, and Vincent [43, 44]. A constant potential of 10 mV was applied to polarise the cells and initial (I_0) and steady state currents (I_{ss}) were measured. The impedance spectra were determined before (R_0) and after experiments (R_{ss}) and Na^+ transference number was measured using the following formula [44]:

$$t_{Na+} = \frac{I_{ss}\,(V - I_0 R_0)}{I_0\,(V - I_{ss} R_{ss})}.$$

A VMP3/Z Multi Potentiostat (Bio-Logic Science Instruments) and EC-Lab software version 11.27 was used for conducting all experiments and fitting the impedance data.

2.5. Synthesis of carbon-coated $Na_3V_2(PO_4)_3$/C (NVP) cathode material

The synthesis of carbon-coated $Na_3V_2(PO_4)_3$ was performed as described elsewhere [32]. Briefly, V_2O_5 (Sigma Aldrich, 99.9%) and H_2C_2O4 (Sigma Aldrich, anhydrous) were dissolved into deionized water and vigorously stirred at 70 °C for 1 h; after this process a VOC_2O_4 solution was obtained. Subsequently, NaH_2PO_4 and glucose were added to the VOC_2O_4 solution and the mixture was kept under vigorous stirring for a further 10 min. Afterwards, N-propanol was added into the VOC_2O_4 solution and this was left stirring for 30 min. The NVP precursor was obtained by removing the solvent by using a rotary evaporator and the obtained solid was further dried under vacuum at 60 °C for 12 h. Finally, $Na_3V_2(PO_4)_3$/C micro-composites were obtained by pre-treating the precursor at 400 °C for 4 h followed by annealing at 750 °C for 8 h under inert atmosphere (Ar) at a heating rate of 5 °C min^{-1}.

2.6. Fabrication of $Na_3V_2(PO_4)_3$/C (NVP) cathode electrodes

NVP cathode electrodes were prepared by making a slurry composed of 80% of active material ($Na_3V_2(PO_4)_3$/C), 10% of PVDF binder (Sigma-Aldrich) and 10% of conductive carbon (C65, Timcal). The slurry was obtained by pre-dissolving the binder in NMP (N-2-methyl-pyrrolidinone) into a small beaker and left stirring. Separately, a pre-weighed amount of NVP cathode material and carbon C65 were ground in an agate mortar for 30 min. Subsequently, the ground solid (NVP + C65) was added to the beaker containing the pre-dissolved binder and a few extra drops of NMP solvent were added to the beaker. In order to obtain a homogeneous slurry, the slurry was left stirring overnight. Finally, the homogeneous slurry was cast onto aluminium foil by using a doctor blade. The NVP/C film was dried at 70 °C under vacuum for 24 h and then punched into disks (0.5 cm^2) to obtain the electrodes. A set of electrodes were weighed and the average mass loading was around 1.5 mg cm^{-2}.

2.7. Assembly of sodium-metal batteries

The Na-NVP full cell was assembled by putting NVP electrode (8 mm in diameter) and Na metal foil (10 mm in diameter) into a coin cell. The membranes (20 mol% NaFSI in $[P_{1i444}][FSI]$ + PVDF, 20 mol% NaTFSI in $[P_{1i444}][FSI]$ + PVDF) acting as both electrolyte and separator, were placed between the anode and cathode. The assembled cells were first rested for 12 h at 70 °C prior to the electrochemical test. The Na-NVP cells were then cycled within the voltage range from 3.8 V to 2.5 V under different current densities. Long-term cycling was conducted at 1/20 C (1 C = 115 mAh g^{-1}) for ten cycles and then at 1/5 C for the duration of the experiment. Rate capability assessment was carried out at 1/20 C, 1/10 C, 1/5 C, 1/2 C, and 1 C subsequently The cycling test was performed using a Neware battery testing system.

3. Results and discussion

3.1. Phase behaviour of the composite electrolytes

Figure 2(a) compares the DSC heating traces of pristine $[P_{1i444}][FSI]$, 20 mol% NaFSI in $[P_{1i444}][FSI]$ and 20 mol% NaFSI doped $[P_{1i444}][FSI]$ cast onto a PVDF nanofibre mat, during the first and second heating

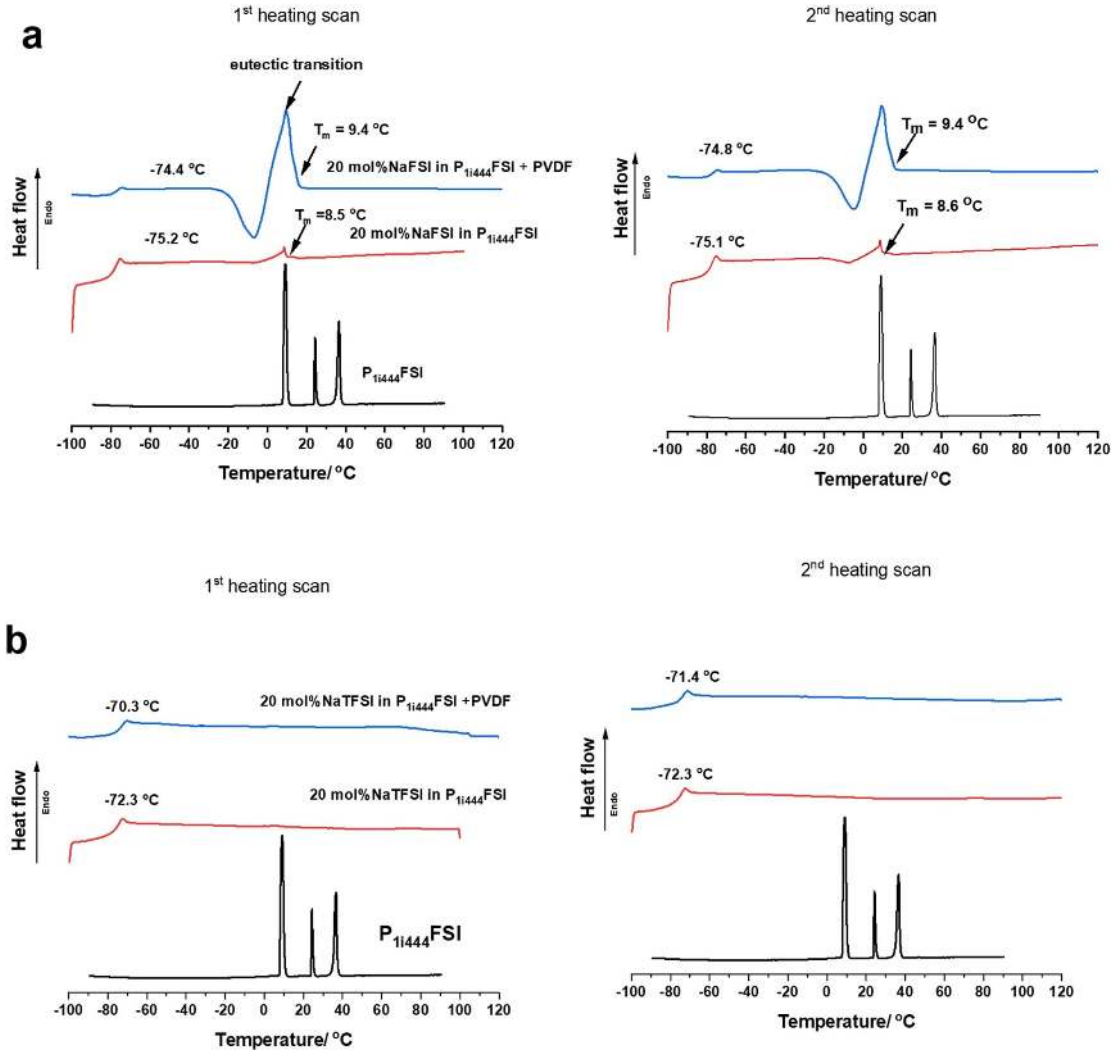

Figure 2. The DSC heating traces 10 °C min^{-1} of (a) $[P_{1i444}][FSI]$, 20 mol% NaFSI in $[P_{1i444}][FSI]$ and its PVDF composite, first and second heating scans. (b) $[P_{1i444}][FSI]$, 20 mol% NaTFSI in $[P_{1i444}][FSI]$ and its PVDF composite, first and second heating scans.

scans. The DSC trace of pristine $[P_{1i444}][FSI]$ shows two solid-solid transitions at 8.9 °C and 24.3 °C and a melt at 36.7 °C. However, on addition of 20 mol% of NaFSI, the solid-solid transition peaks of $[P_{1i444}][FSI]$ disappear which is consistent with loss of crystallinity, and likely presence of a liquid phase formed in the binary system, and has been discussed in previous work [28]. Given that the melting peak of $[P_{1i444}][FSI]$ decreases from 37 °C to 8.5 °C with very small entropy of fusion, the material melts before the solid–solid phase transitions seen in the pure OIPC can occur. Furthermore, a large T_g along with visual appearance is evident in these mixtures confirming that the materials are liquids, however, these are clearly metastable liquids, since a cold crystallisation is observed on heating just before the melting peak. Interestingly, prior to melting, the binary system crystallises which suggests that the sample does not freeze instantly on cooling and remains in the supercooled liquid state. In the OIPC/PVDF composite electrolyte, the cold crystallisation and subsequent melting peak are significantly larger, indicating that the PVDF fibre surfaces act as a nucleation site to encourage the crystallisation on heating, whereas in the absence of the fibres this process is more sluggish and the melt occurs before much of the material can crystallise. The interaction with the PVDF fibre surface is also evident by the slight increase in T_g from −75.2 °C in the 20 mol% NaFSI doped $[P_{1i444}][FSI]$ to −74.4 °C in the presence of PVDF.

In the mixtures of $[P_{1i444}][FSI]$ with 20 mol% NaTFSI, the solid-solid transition peaks as well as the melting peak of $[P_{1i444}][FSI]$ completely disappear, as presented in figure 2(b), with the sample remaining as an IL over the whole temperature range and displaying a T_g at −72.3 °C. Interestingly, in the first scan and in the presence of PVDF fibres, a broad transition (across 50 °C–100 °C) can just be made out in the DSC trace, which disappears on the second scan. An increase in T_g is also seen in this mixed anion electrolyte, shifting from −72.3 °C in the bulk liquid to −70.3 °C in the self-standing membrane. It is interesting that the

Table 1. Na ion transport number, ionic conductivity and corresponding Na ion conductivity at 50 °C.

	Na^+ transference number	Ionic conductivity (S cm^{-1})	Na ion conductivity (S cm^{-1})
20 mol% NaFSI/[P_{1i444}][FSI]/PVDF	0.21 ± 0.03	$2.1 \times 10^{-3} \pm 0.05 \times 10^{-3}$	4.4×10^{-4}
20 mol% NaTFSI/[P_{1i444}][FSI]/PVDF	0.22 ± 0.09	$2.5 \times 10^{-3} \pm 0.05 \times 10^{-3}$	5.5×10^{-4}

interactions with the PVDF in the case of FSI encourage the crystallisation of the OIPC material whereas in the TFSI salt system the opposite is seen. In contrast, previous work has suggested a stronger polymer–anion interaction in the case of the more fluorine rich TFSI systems [45, 46].

3.2. Sodium-ion transference number and ionic conductivity

The ionic conductivity of the composite electrolytes was calculated by extracting the bulk electrolyte resistance from EIS measurements of sodium symmetrical cells at 50 °C and is presented in table 1. The ionic conductivity value of the 20 mol% NaFSI in [P_{1i444}][FSI] at 50 °C was slightly higher (2.5×10^{-3} S cm^{-1}) than that of 20 mol% NaTFSI in [P_{1i444}][FSI] (2×10^{-3} S cm^{-1}) [38]. However, in the composite electrolyte the ionic conductivity of the 20 mol% NaFSI/[P_{1i444}][FSI]/PVDF is slightly lower (2.1×10^{-3} S cm^{-1}) than the 20 mol% NaTFSI/[P_{1i444}][FSI]/PVDF (2.5×10^{-3} S cm^{-1}). This observation can be attributed to the different interactions of the FSI^- and $TFSI^-$ anions with PVDF. $TFSI^-$ has strong dipole–dipole interactions with PVDF which leads to the formation of a highly conductive layer at the interphase between the electrolyte and PVDF for Na ion transport [47]. Thus, PVDF nanofibers do not only provide structural support for creating free-standing membranes from the liquid electrolyte, but also, interacts with the NaTFSI-doped electrolyte, making it more conductive [46]. On the other hand, the FSI^- anion interacts weakly with PVDF. This is also consistent with the phase behaviour discussed above indicates PVDF promotes crystallisation of the NaFSI containing OIPC. This is similar to observation made by Zhou *et al* where adding Li–C_2mpyrFSI to PVDF nanofibers led to a decrease in ionic conductivity [22].

The effective sodium ion conductivity in the composite electrolytes was calculated from the transference number. The transference number measurements were conducted by applying a small constant voltage and recording the initial and steady-state currents together with EIS measurements before and after the polarisation. The change in interfacial resistance before and after the polarisation is negligible because of the stability of the composite electrolyte towards the Na metal. Figure 3 shows the polarisation and EIS data of the two composite electrolytes. The transference number was calculated to be 0.21 ± 0.03 for the 20 mol% NaFSI/[P_{1i444}][FSI]/PVDF and 0.22 ± 0.09 for the 20 mol% NaTFSI/[P_{1i444}][FSI]/PVDF samples. Based on these values, along with the total ionic conductivity at 50 °C for the samples, the Na ion conductivity was also calculated and presented in table 1. In general, the Na ion conductivity in both samples is high, compared to the bulk electrolyte (20 mol% NaFSI or NaTFSI in [P_{1i444}][FSI], and other gel polymer electrolytes reported in the literature [48–50], indicating these solid electrolytes may be feasible for further investigation in a full cell. However, the Na ion conductivity in the NaTFSI/[P_{1i444}][FSI]/PVDF electrolyte is slightly higher than the NaFSI/[P_{1i444}][FSI]/PVDF composite, which may offer advantages in delivering marginally higher specific capacity as is demonstrated below.

3.3. Cycling stability of sodium symmetrical cells

To study the compatibility of the composite electrolytes with the reactive sodium metal and the ability of the electrolyte to support sodium electrochemistry, Na symmetrical cells were fabricated. Figures 4(a) and (c) show the galvanostatic cycling of sodium symmetrical cells of 20 mol% NaFSI/[P_{1i444}][FSI]/PVDF and 20 mol% NaTFSI/[P_{1i444}][FSI]/PVDF at 50 °C by applying various current densities ranging from 0.05 mA cm^{-2} to 0.5 mA cm^{-2} and a polarization interval of 1 h. As can be seen in figure 3(a), a low and stable polarization potential (12 mV at 0.05 mA cm^{-2} and 90 mV at 0.5 mA cm^{-2} is observed in the 20 mol% FSI/[P_{1i444}][FSI]/PVDF sample. A lower polarisation potential of 10 mV was achieved when 0.05 mA cm^{-2} was again applied after cycling at a higher current density (0.5 mA cm^{-2}). These overpotential values are slightly lower (25 mV at 0.1 mA cm^{-2}) than the same material (20 mol% NaFSI in [P_{1i444}][FSI]) in a glass fibre separator [38]. Furthermore, the stable cycling is comparable to the 50 mol% NaFSI in [P_{111i4}][FSI] with a Solupor separator [51]. A cell polarization of 15 mV was observed at relatively low current density (0.05 mA cm^{-2}) in the TFSI system. Increasing the current density to 0.5 mA cm^{-2} resulted in a short circuit after two cycles. The underlying reason of this behaviour is under investigation.

Electrochemical impedance spectroscopy (EIS) measurements were conducted after each applied current density (after every five cycles) to obtain a better understanding of the cycling behaviour. The Nyquist plots are presented in figures 4(b) and (d) and the Bode plots (amplitude and phase angle), in figure S2. The EIS

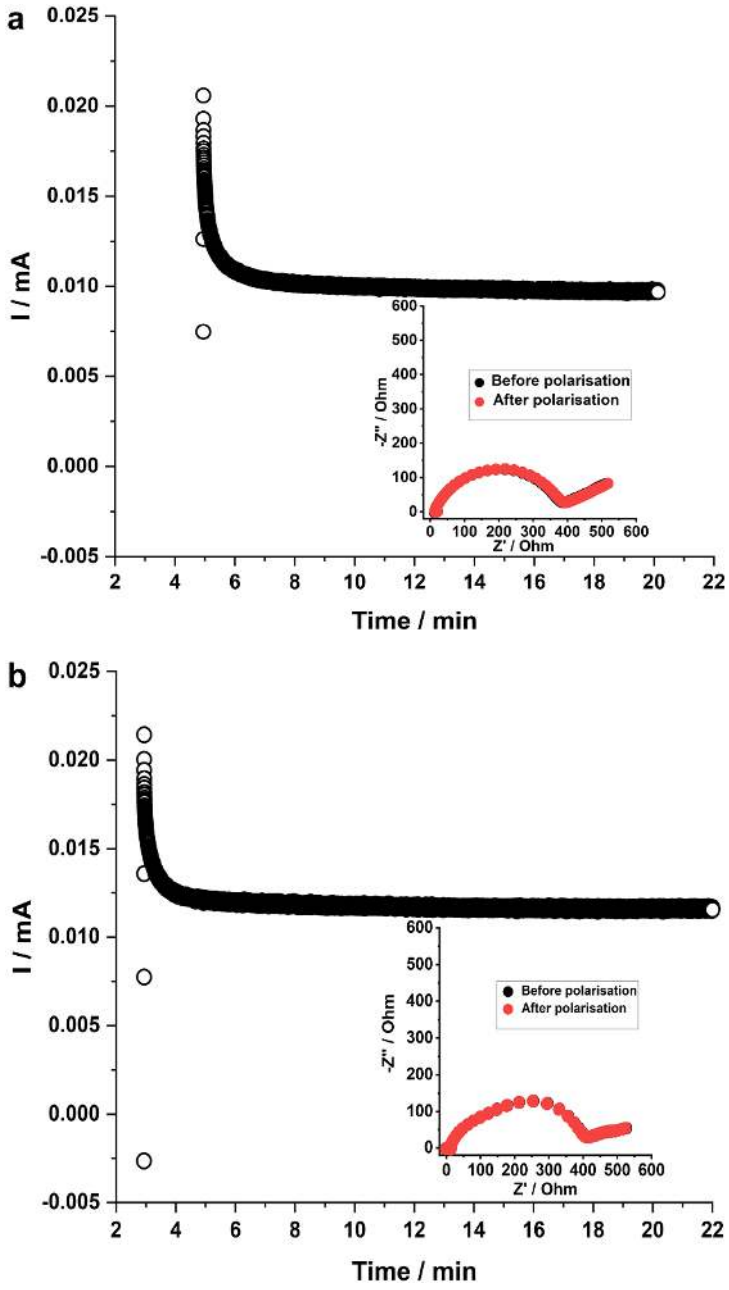

Figure 3. (a) Current vs time upon applying small voltage of 10 mV at 50 °C to (a) 20 mol% NaFSI/[P_{1i444}][FSI]/PVDF (b) of 20 mol% NaTFSI/[P_{1i444}][FSI]/PVDF. Electrochemical impedance spectra of the cells before and after polarization.

data were fitted with equivalent electric circuits. The fitting results are presented in the supporting information (table S1). The Nyquist plots of the cells with fitted impedance spectra after 20 cycles (after 0.3 mA cm^{-2} applied current density) and an equivalent circuit for that spectrum (as an example) are presented in figure S3. The best fits were achieved when employing a two-component layer model using constant phase elements (CPEs) with a Warburg diffusion component. CPEs are used to describe the real system that contains both capacitance and resistance. Based on the equivalent circuit model, the Nyquist plots show that the impedance spectra consists of two semicircles. R_b is the bulk resistance of the composite electrolyte and $Z_{\text{charge transfer (ct)}}$ is the impedance related to charge transfer and ion diffusion at the surface of the sodium metal. The second semicircle is $Z_{\text{interfacial (int)}}$, the impedance of the passivation layer formed on the surface of the sodium metal, which involves the resistance of that layer (R_{int}) and its related CPE (CPE_{int}).

The initial overall cell resistance decreased from 800 ± 30 Ω after the 5th cycle to 415 ± 12 Ω after the 25th cycle (after applying 0.5 mA cm^{-2}) in the 20 mol% NaFSI/[P_{1i444}][FSI]/PVDF electrolyte. Whereas for the NaTFSI sample the cell resistance was slightly reduced from 600 ± 15 Ω after the 5th cycle to 447 ± 12 Ω after the 25th cycle. The decrease in the cell resistance for the FSI system may indicate that a stable and ion-conductive SEI layer forms upon successive cycling.

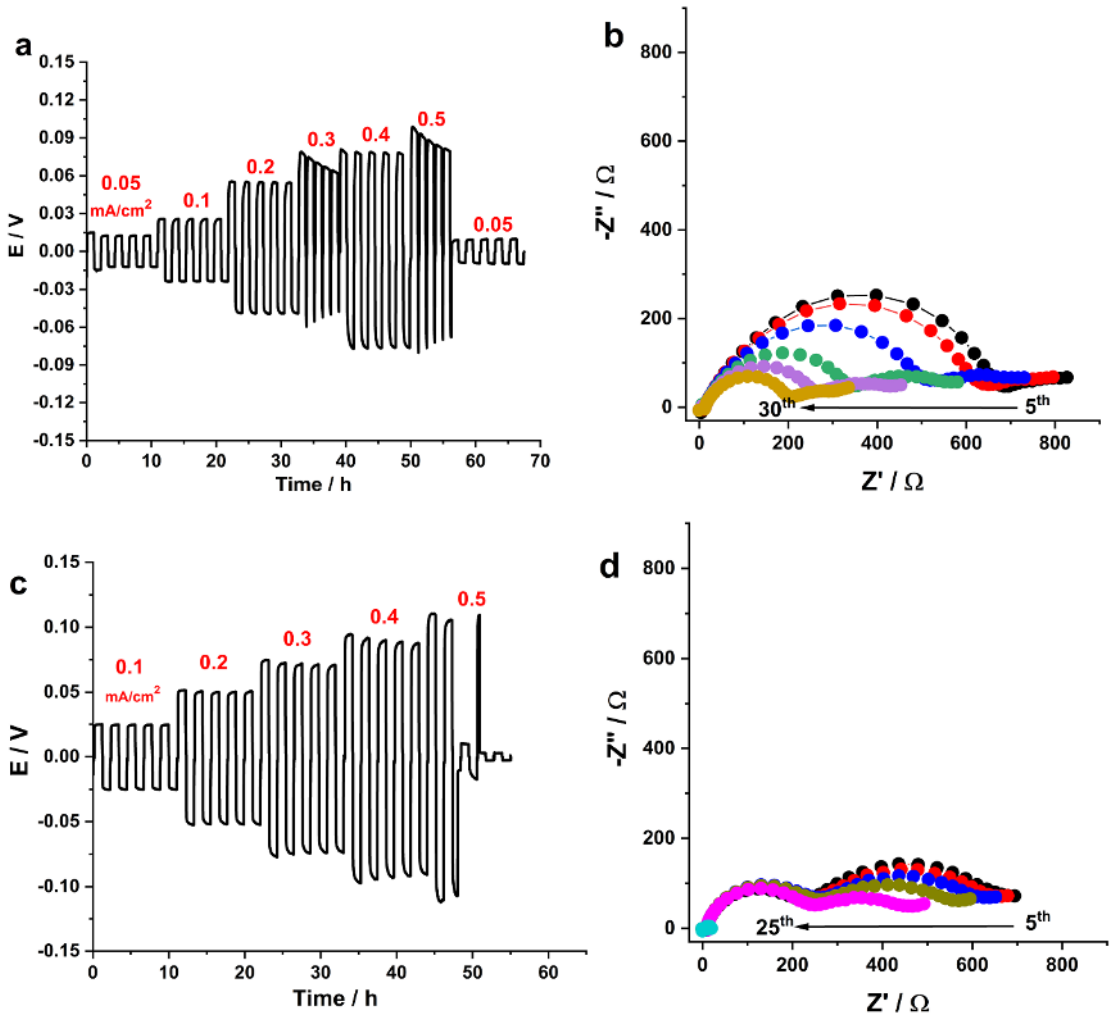

Figure 4. (a) Symmetric coin cell cycling of 20 mol% NaFSI/[P_{1i444}][FSI]/PVDF at various current densities (0.05 mA cm^{-2}–0.5 mA cm^{-2}). (b) The Nyquist plots of this cell after every five cycles. (c) Symmetric coin cell cycling of 20 mol% NaTFSI/[P_{1i444}][FSI]/PVDF at various current densities. (d) Selected Nyquist plots obtained after every five cycles. Cells were cycled at 50 °C with 1 h stripping and 1 h plating time.

The differences in the electrode/electrolyte interface with the different composites can clearly be seen in figure S2, where the Bode plots corresponding to figures 4(b) and (d) are presented. Both cells exhibit a very similar high frequency impedance, which indicates their ionic conductivity is very similar as the bulk electrolyte resistance is probed at these high frequencies. At frequencies below 10^3 Hz, however, the symmetric cell with the TFSI/[P_{1i444}][FSI]/PVDF membrane exhibited a stable impedance without any significant changes upon increasing the current densities. In the case of the FSI/[P_{1i444}][FSI]/PVDF composite, at frequencies below 10^3 Hz, the impedance decreased with increasing the applied current density, indicating the interfacial resistance changed to lower values by increasing the current density. By applying higher current densities, the morphology and composition of the SEI layer may change to form a more uniform and homogeneous passivation layer. Moreover, as reported recently in the case of Li metal cells [52], at higher current densities, fluorinated anions (FSI^- and $TFSI^-$) and Na^+ can reach to the interface close to the Na metal electrode. These anions will be then reduced to form a stable SEI layer enriched in NaF components. Rakov *et al* also reported the formation of $Na_x(FSI)_y$ molten salt-like nanostructured interfacial layer at the surface of electrode once larger overpotentials are applied by simulating 50 mol% NaFSI in [C_3mpyr][FSI] electrolyte [53]. However, to understand the SEI composition and morphology in detail further surface analysis are under investigation.

Longer-term symmetrical cell cycling was conducted at 50 °C for both 20 mol% NaFSI/[P_{1i444}][FSI]/PVDF and 20 mol% NaTFSI/[P_{1i444}][FSI]/PVDF, after resting at that temperature for 24 h, with 1 h interval for 100 cycles (figure 5(a)). In general, stable stripping and plating was observed for both systems with a low overpotential for more than 100 cycles without any break down. Initially the overpotential for the

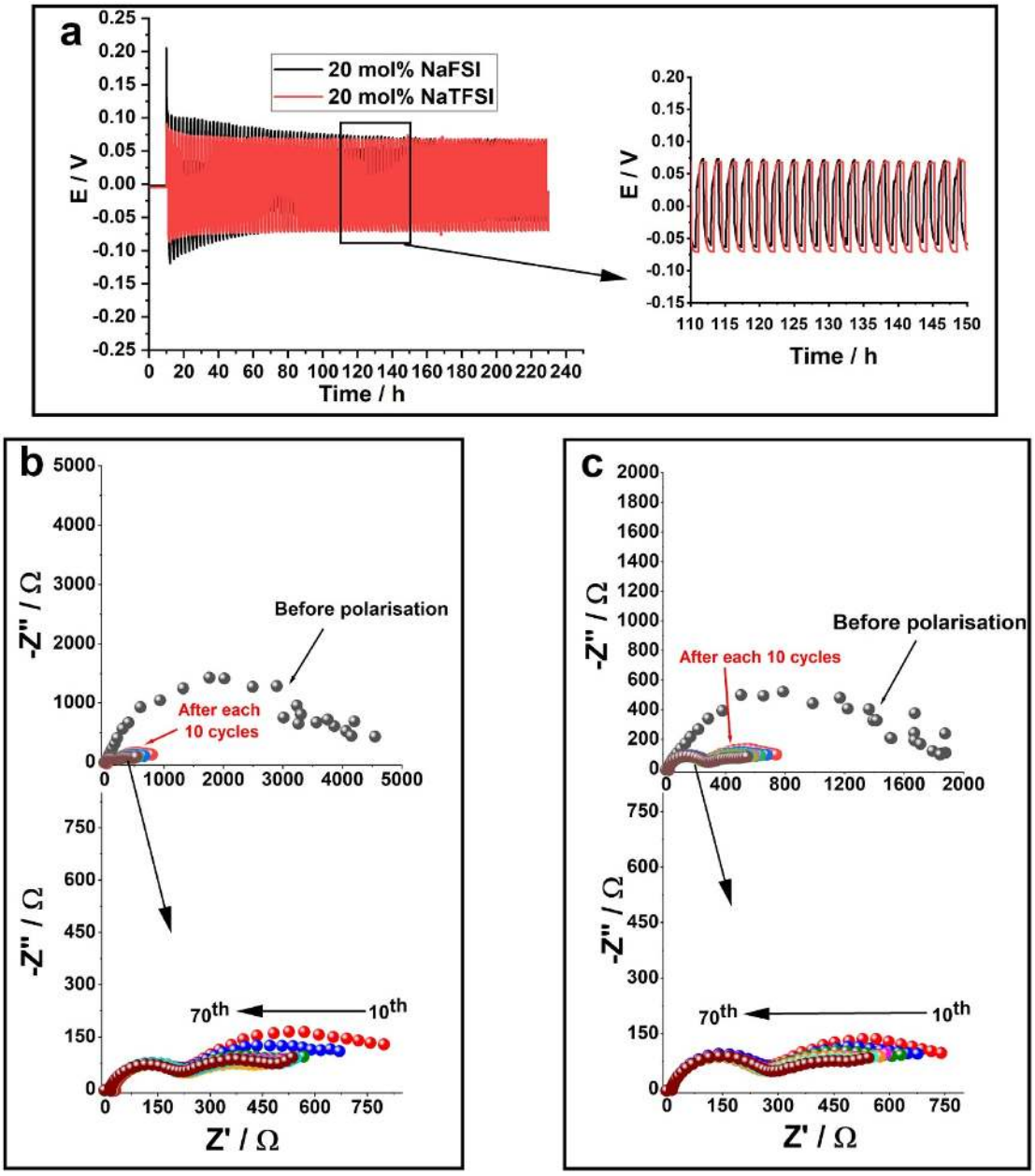

Figure 5. (a) Voltage-time profile of long-term cycling of Na symmetrical cells with 20 mol% NaFSI/[P_{1i444}][FSI]/PVDF and 20 mol% NaTFSI/[P_{1i444}][FSI]/PVDF at 0.2 mA cm^{-2} applied current density and 1 h interval for stripping and plating at 50 °C. (b) EIS data extracted before polarisation and after each ten cycles for 20 mol% NaFSI/[P_{1i444}][FSI]/PVDF. (c) EIS data extracted before polarisation and after each ten cycles for 20 mol% NaTFSI/[P_{1i444}][FSI]/PVDF.

FSI system was high, 200 mV, and decreased upon continued cycling to ≈70 mV after 50 cycles, reaching values similar to the TFSI system and remaining stable thereafter.

The compatibility of these electrolytes with sodium metal was also studied by monitoring the impedance change of the Na|Na cells at 50 °C. The Nyquist and Bode plots of the cells before cycling and after each ten cycles are presented in figures 5(b), (c) and S4(a), (b). The impedance data were fitted with the same two-component circuit model described previously and the R_{int}, R_{ct}, CPE_{int} and CPE_{ct} values are shown in table S3 to S6 after 10 and 50 cycles. An example of a fitted Nyquist spectrum after the 50th cycle is presented in figure S5. Before cycling, the cell resistance values for the FSI and TFSI systems were 4200 ± 70 and 1860 ± 50 Ω respectively. However, after ten cycles the resistance of SEI layer decreased to 508 ± 20 Ω for the composite with NaFSI and 483 ± 20 Ω for the composite with NaTFSI. This demonstrates the evolution of the interphase and that ten stripping/plating cycles is enough to create a stable and ion-conductive SEI layer. The interfacial resistances are close in both NaFSI and NaTFSI systems after 50 cycles, which is in good agreement with the higher polarisation potential with the NaFSI electrolyte during the first 50 cycles before stabilising (figure 5).

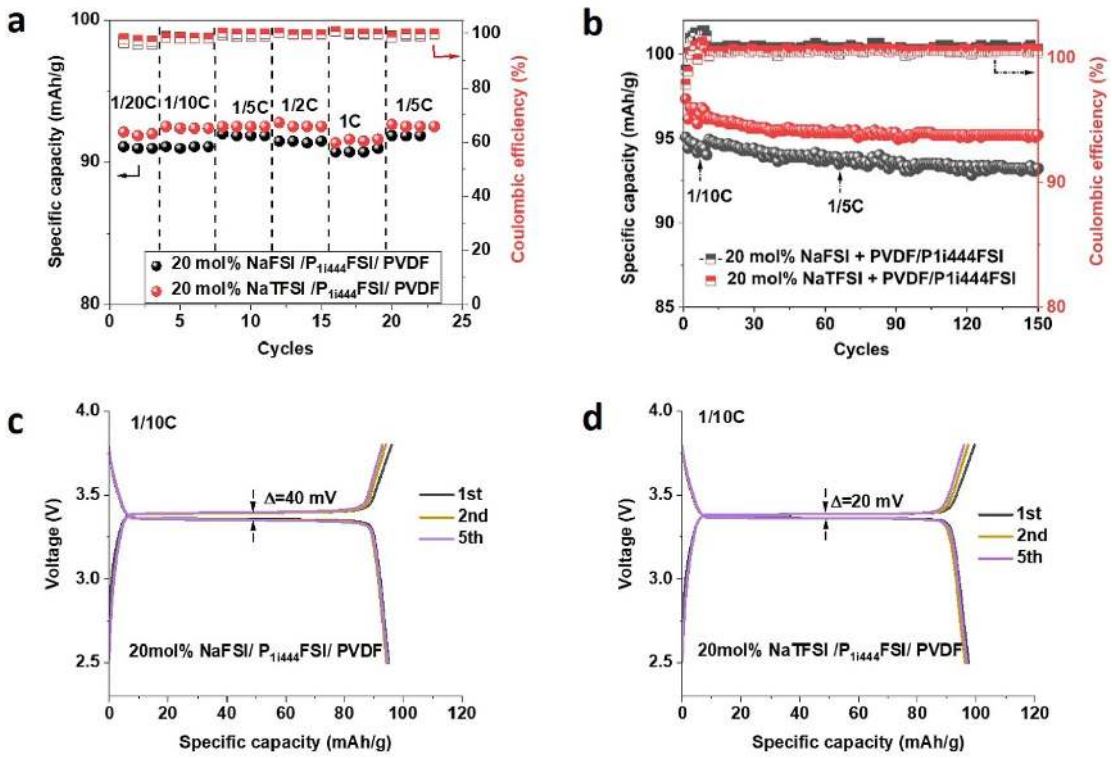

Figure 6. (a) The rate performance of NVP/C |20 mol% NaFSI/[P_{1i444}][FSI]/PVDF|Na and NVP/C|20 mol% NaTFSI/[P_{1i444}][FSI]/PVDF |Na batteries at 50 °C at current rates of C/20, C/10, C/5, C/2 and C. (b) Cycling performance of the cells at 50 °C. (c) The charge/discharge curves of NVP/C |20 mol% NaFSI/[P_{1i444}][FSI]/PVDF |Na at a current rate of C/10. (d) The charge/discharge curves of NVP/C |20 mol% NaTFSI/[P_{1i444}][FSI]/PVDF |Na at a current rate of C/10.

The decrease in the interfacial resistance upon cycling is more obvious in the Bode plots in figure S4. The impedance at lower frequency is related to the interfacial and charge transfer impedance, and is nearly two orders of magnitude larger in the NaFSI system, prior to cycling compared with after the 10th cycle, and an order of magnitude larger in the equivalent NaTFSI case. The drop in the interfacial resistance at higher frequency is greater in the NaFSI system compared to the NaTFSI case, which accounts for the drop in overpotential in the FSI/[P_{1i444}][FSI]/PVDF system with cycling.

3.4. Na/$Na_3V_2(PO_4)_3$ cell cycling performance

The cycling performance of the PVDF composite electrolytes with 20 mol% NaFSI in [P_{1i444}][FSI] and 20 mol% NaTFSI in [P_{1i444}][FSI] were then studied in a rechargeable sodium-metal coin cell at 50 °C, using a sodium vanadium phosphate–carbon composite ($Na_3V_2(PO_4)_3$) (NVP/C) based cathode material with a theoretical capacity of 118 mAh g^{-1}. Rate capability performance was tested at different current rates between C/20 and C, and presented in figure 6(a). These results show a remarkable rate capability of the cell, delivering reversible capacity of 91.0 and 90.7 mAh g^{-1} at rate of C/20 and 1 C for 20 mol% NaFSI/[P_{1i444}][FSI]/PVDF and 92 and 91.3 for a cell containing 20 mol% NaTFSI/[P_{1i444}][FSI]/PVDF samples. When the current density returned to C/5 after cycling at a higher rate of 1 C, the capacity of 91.9 and 92.6 mAh g^{-1} for the cells with 20 mol% NaFSI/[P_{1i444}][FSI]/PVDF and 20 mol% NaTFSI/[P_{1i444}][FSI]/PVDF, respectively, was recovered. The long term cycling of NVP/C|20 mol% NaFSI/[P_{1i444}][FSI]/PVDF|Na and NVP/C|20 mol% NaTFSI/[P_{1i444}][FSI]/PVDF|Na was also performed at 50 °C. Both cells exhibited stable long term cycling at C/5 at 50 °C, as shown in figure 6(b). A capacity of 93 and 95 mAh g^{-1} with a 98.0% and 98.5% capacity retention over 150 cycles for cells containing 20 mol% NaFSI and 20 mol% NaTFSI respectively was delivered. Their performance is better than NVP/C|[C_3mpyr][FSI]/NaTFSI/PVDF − HFP) |Na cell that shows 92% capacity retention at room temperature at C/10 after 300 cycles [50]. The specific capacity is also higher than Na/PEO–Na/NVP cells, which delivered 67.5 mAh g^{-1} at C/2 at room temperature after 100 cycles [54], while cycling of a Na metal cell using a polymer electrolyte based on PEO–$NaClO_4$–Al_2O_3 and NVP cathode results in an initial capacity of 96 mAh g^{-1} at 2 C at 80 °C [55]. The results here are also comparable with the cycling of Na–metal cell based on an NVP cathode and an EC + DEC liquid electrolyte with 1 M NaFSI which showd a specific capacity of 99.5 mAh g^{-1} after 80 cycles at a rate of C/10 at room temperature [56]. However, such organic solvent based electrolytes show substantial

capacity decay [27] along with imposing additional safety issues at an elevated operating temperature which is required for extreme climate condition and applications where elevated temperatures are required. In such cases the higher temperature operation and stability is critical. Figures 6(c) and (d) shows the voltage profiles for NVP/C|20 mol% NaFSI/[P_{1i444}][FSI]/PVDF|Na and NVP/C|20 mol% NaTFSI/[P_{1i444}][FSI]/PVDF|Na cells at a rate of C/10. The polarisation of the cell containing 20 mol% NaTFSI was less (20 mV) than that with NaFSI (40 mV), indicative of the lower overall resistance of the cell prepared with mixed anion based composite, which is also consistent with the slightly higher ionic conductivity of 20 mol% NaTFSI/[P_{1i444}][FSI]/PVDF reported in table 1. We demonstrate Na batteries for high temperature applications with high cycling stability and rate capability based on the safe and stable polymer/OIPC composite electrolyte combined with the economically feasible cathode material namely NVP/C that propose high-level performance.

4. Conclusion

Solid-state composite electrolyte membranes based on the OIPC [P_{1i444}][FSI] with 20 mol% NaFSI or NaTFSI and PVDF nanofiber mats have been prepared and characterised. The thermal analysis data indicates that PVDF encourages crystallisation of the NaFSI/P_{1i44}FSI mixture in the solid-state whereas an amorphous electrolyte is retained in the NaTFSI/[P_{1i444}][FSI] mixture. The ionic conductivity of the NaTFSI/[P_{1i444}][FSI]/PVDF composite is slightly higher than for the NaFSI/[P_{1i444}][FSI]/PVDF composite leading to a marginally lower polarisation during cell cycling. Stable Na symmetric cell cycling was obtained with low polarisation potential (≈70 mV) for NaTFSI/[P_{1i444}][FSI]/PVDF sample over 100 cycles at 0.2 mAh g^{-1}. However, a longer cycling period was required to stabilise the cell containing the NaFSI/[P_{1i444}][FSI]/PVDF membrane; this could be due to the SEI layer stabilisation or possibly the initial greater ordering in this latter system as was suggested from the thermal analysis. Na|NVP/C full cells were fabricated and cycled with high stability at C/5 and 50 °C, with a reversible capacity of 94 and 95 mAh g^{-1} for 20 mol% NaFSI/[P_{1i444}][FSI]/PVDF and NaTFSI/[P_{1i444}][FSI]/PVDF composite electrolytes respectively, after 60 cycles. The full cells exhibit excellent C-rate capability with a reversible discharge capacity of above 90 mAh g^{-1} even at 1 C and 50 °C. The mixed anion systems appear to outperform the composite electrolyte containing only FSI, which appears to be related to electrolyte interactions with the PVDF fibres and will be further explored in future work. The cycling performances for both systems is encouraging and suggests that, even though the OIPC cation is relatively large compared with the smaller P_{111i4} previously studied, it does not impede the performance of these solid state membranes in a Na battery. From a commercial perspective this alternative cation is beneficial as the larger phosphonium cations are easier and more cost effective to prepare.

Data availability statement

All data that support the findings of this study are included within the article (and any supplementary files).

Acknowledgments

The authors would like to acknowledge the Australian Research Council Centre of Excellence for Electromaterials Science (ACES) for funding through CE140100012.

Conflict of interest

The authors declare no actual or potential conflict of interest including any financial and personal relationships with other people or organizations.

ORCID iD

Faezeh Makhlooghiazad https://orcid.org/0000-0002-8002-9668

References

[1] Chayambuka K, Mulder G, Danilov D L and Notten P H L 2018 Sodium-ion battery materials and electrochemical properties reviewed *Adv. Energy Mater.* **8** 1800079–128
[2] Sawicki M and Shaw L L 2015 Advances and challenges of sodium ion batteries as post lithium ion batteries *RSC Adv.* **5** 53129–54
[3] Yabuuchi N, Kubota K, Dahbi M and Komaba S 2014 Research development on sodium-ion batteries *Chem. Rev.* **114** 11636–82
[4] Slater M D, Kim D, Lee E and Johnson C S 2013 Sodium-ion batteries *Adv. Funct. Mater.* **23** 947–58
[5] Bauer A, Song J, Vail S, Pan W, Barker J and Lu Y 2018 The scale-up and commercialization of nonaqueous Na-ion battery technologies *Adv. Energy Mater.* **8** 1702869–82

[6] Kundu D, Talaie E, Duffort V and Nazar L F 2015 The emerging chemistry of sodium ion batteries for electrochemical energy storage *Angew. Chem., Int. Ed. Engl.* **54** 3431–48
[7] Hwang J Y, Myung S T and Sun Y K 2017 Sodium-ion batteries: present and future *Chem. Soc. Rev.* **46** 3529–614
[8] Goodenough J B and Kim Y 2011 Challenges for rechargeable batteries *J. Power Sources* **196** 6688–94
[9] Bhatt A I, Best A S, Huang J and Hollenkamp A F 2010 Application of the N–propyl–N–methyl-pyrrolidinium bis(fluorosulfonyl) imide RTIL containing lithium bis(fluorosulfonyl)imide in ionic liquid based lithium batteries *J. Electrochem. Soc.* **157** A66–74
[10] Zhang Z *et al* 2018 New horizons for inorganic solid state ion conductors *Energy Environ. Sci.* **11** 1945–76
[11] De Anastro A F, Lago N, Berlanga C, Galcerán M, Hilder M, Forsyth M and Mecerreyes D 2019 Poly(ionic liquid) iongel membranes for all solid-state rechargeable sodium battery *J. Membr. Sci.* **582** 435–41
[12] Forsyth M, Chimdi T, Seeber A, Gunzelmann D and Howlett P C 2014 Structure and dynamics in an organic ionic plastic crystal, N–ethyl–N–methyl pyrrolidinium bis(trifluoromethanesulfonyl) amide, mixed with a sodium salt *J. Mater. Chem.* A **2** 3993–4003
[13] Xu C *et al* 2020 Reversible hybrid sodium-CO_2 batteries with low charging voltage and long-life *Nano Energy* **68** 104318–26
[14] Cheng M, Qu T, Zi J, Yao Y, Liang F, Ma W, Yang B, Dai Y and Lei Y 2020 A hybrid solid electrolyte for solid-state sodium ion batteries with good cycle performance *Nanotechnology* **31** 425401
[15] Makhlooghiazad F, Gunzelmann D, Hilder M, MacFarlane D R, Armand M, Howlett P C and Forsyth M 2017 Mixed phase solid-state plastic crystal electrolytes based on a phosphonium cation for sodium devices *Adv. Energy Mater.* **7** 1601272–81
[16] Tian S, Shao B, Wang Z, Li S, Liu X, Zhao Y and Li L 2019 Organic ionic plastic crystal as electrolyte for lithium-oxygen batteries *Chin. Chem. Lett.* **30** 1289–92
[17] Yang K, Liao Z, Zhang Z, Yang L and Hirano S-I 2019 Ionic plastic crystal-polymeric ionic liquid solid-state electrolytes with high ionic conductivity for lithium ion batteries *Mater. Lett.* **236** 554–7
[18] Zhou Z-B and Matsumoto H 2007 Lithium-doped, organic ionic plastic crystal electrolytes exhibiting high ambient-temperature conductivities *Electrochem. Commun.* **9** 1017–22
[19] Jin L, Nairn K M, Forsyth C M, Seeber A J, MacFarlane D R, Howlett P C, Forsyth M and Pringle J M 2012 Structure and transport properties of a plastic crystal ion conductor: diethyl(methyl)(isobutyl)phosphonium hexafluorophosphate *J. Am. Chem. Soc.* **134** 9688–97
[20] Park C B and Sung B J 2020 Heterogeneous rotational dynamics of imidazolium-based organic ionic plastic crystals *J. Phys. Chem.* B **124** 6894–904
[21] Goossens K, Rakers L, Heinrich B, Ahumada G, Ichikawa T, Donnio B, Shin T J, Bielawski C W and Glorius F 2019 Anisotropic, organic ionic plastic crystal mesophases from persubstituted imidazolium pentacyanocyclopentadienide salts *Chem. Mater.* **31** 9593–603
[22] Zhou Y, Wang X, Zhu H, Yoshizawa-Fujita M, Miyachi Y, Armand M, Forsyth M, Greene G W, Pringle J M and Howlett P C 2017 Solid-state lithium conductors for lithium metal batteries based on electrospun nanofiber/plastic crystal composites *ChemSusChem* **10** 3135–45
[23] Zhou Y, Wang X, Zhu H, Armand M, Forsyth M, Greene G W, Pringle J M and Howlett P C 2017 N-ethyl-N-methylpyrrolidinium bis(fluorosulfonyl)imide-electrospun polyvinylidene fluoride composite electrolytes: characterization and lithium cell studies *Phys. Chem. Chem. Phys.* **19** 2225–34
[24] Jin L, Howlett P, Efthimiadis J, Kar M, Macfarlane D and Forsyth M 2011 Lithium doped N,N-dimethyl pyrrolidinium tetrafluoroborate organic ionic plastic crystal electrolytes for solid state lithium batteries *J. Mater. Chem.* **21** 10171–8
[25] Biernacka K, Al-Masri D, Yunis R, Zhu H, Hollenkamp A F and Pringle J M 2020 Development of new solid-state electrolytes based on a hexamethylguanidinium plastic crystal and lithium salts *Electrochim. Acta* **357** 136863–74
[26] Wang X, Kerr R, Chen F, Goujon N, Pringle J M, Mecerreyes D, Forsyth M and Howlett P C 2020 Toward high-energy-density lithium metal batteries: opportunities and challenges for solid organic electrolytes *Adv. Mater.* **32** e1905219
[27] Makhlooghiazad F, Sharma M, Zhang Z, Howlett P C, Forsyth M and Nazar L F 2020 Stable high-temperature cycling of Na metal batteries on Na3V2(PO4)3 and Na2FeP2O7 cathodes in NaFSI-rich organic ionic plastic crystal electrolytes *J. Phys. Chem. Lett.* **11** 2092–100
[28] Makhlooghiazad F, Howlett P C, Wang X, Hilder M, MacFarlane D R, Armand M and Forsyth M 2017 Phosphonium plastic crystal salt alloyed with a sodium salt as a solid-state electrolyte for sodium devices: phase behaviour and electrochemical performance *J. Mater. Chem.* A **5** 5770–80
[29] Yang H, Hwang J, Wang Y, Matsumoto K and Hagiwara R 2019 N–Ethyl–N–propylpyrrolidinium bis(fluorosulfonyl)amide ionic liquid electrolytes for sodium secondary batteries: effects of Na ion concentration *J. Phys. Chem.* C **123** 22018–26
[30] Yoshii K, Yamaji K, Tsuda T, Tsunashima K, Yoshida H, Ozaki M and Kuwabata S 2013 Physicochemical properties of tri-n-butylalkylphosphonium cation-based room-temperature ionic liquids *J. Phys. Chem.* B **117** 15051–9
[31] Armel V, Forsyth M, MacFarlane D R and Pringle J M 2011 Organic ionic plastic crystal electrolytes; a new class of electrolyte for high efficiency solid state dye-sensitized solar cells *Energy Environ. Sci.* **4** 2234–9
[32] Mendes T C, Zhang X, Wu Y, Howlett P C, Forsyth M and Macfarlane D R 2019 Supported ionic liquid gel membrane electrolytes for a safe and flexible sodium metal battery *ACS Sustain. Chem. Eng.* **7** 3722–6
[33] Correia D M, Fernandes L C, Martins P M, García-Astrain C, Costa C M, Reguera J and Lanceros-Méndez S 2020 Ionic liquid–polymer composites: a new platform for multifunctional applications *Adv. Funct. Mater.* **30** 1909736–79
[34] Li X, Zhang Z, Li S, Yang L and Hirano S I 2016 Polymeric ionic liquid-plastic crystal composite electrolytes for lithium ion batteries *J. Power Sources* **307** 678–83
[35] Zhang S Y, Zhuang Q, Zhang M, Wang H, Gao Z, Sun J K and Yuan J 2020 Poly(ionic liquid) composites *Chem. Soc. Rev.* **49** 1726–55
[36] Wang X, Girard G M A, Zhu H, Yunis R, MacFarlane D R, Mecerreyes D, Bhattacharyya A J, Howlett P C and Forsyth M 2019 Poly(ionic liquid)s/electrospun nanofiber composite polymer electrolytes for high energy density and safe Li metal batteries *ACS Appl. Energy Mater.* **2** 6237–45
[37] Wang X, Zhu H, Greene G W, Zhou Y, Yoshizawa-Fujita M, Miyachi Y, Armand M, Forsyth M, Pringle J M and Howlett P C 2017 Organic ionic plastic crystal-based composite electrolyte with surface enhanced ion transport and its use in all-solid-state lithium batteries *Adv. Mater. Technol.* **2** 1700046–52
[38] Makhlooghiazad F, Yunis R, Mecerreyes D, Armand M, Howlett P C and Forsyth M 2017 Comparison of the physicochemical and electrochemical behaviour of mixed anion phosphonium based OIPCs electrolytes for sodium batteries *Solid State Ion.* **312** 44–52
[39] Forsyth M, Hilder M, Zhang Y, Chen F, Carre L, Rakov D A, Armand M, Macfarlane D R, Pozo-Gonzalo C and Howlett P C 2019 Tuning sodium interfacial chemistry with mixed-anion ionic liquid electrolytes *ACS Appl. Mater. Interfaces* **11** 43093–106

[40] Hilder M, Gras M, Pope C R, Kar M, MacFarlane D R, Forsyth M and O'Dell L A 2017 Effect of mixed anions on the physicochemical properties of a sodium containing alkoxyammonium ionic liquid electrolyte *Phys. Chem. Chem. Phys.* **19** 17461–8
[41] Wongittharom N, Wang C H, Wang Y C, Yang C H and Chang J K 2014 Ionic liquid electrolytes with various sodium solutes for rechargeable Na/$NaFePO_4$ batteries operated at elevated temperatures *ACS Appl. Mater. Interfaces* **6** 17564–70
[42] Armel V, Velayutham D, Sun J, Howlett P C, Forsyth M, MacFarlane D R and Pringle J M 2011 Ionic liquids and organic ionic plastic crystals utilizing small phosphonium cations *J. Mater. Chem.* **21** 7640–50
[43] Vincent C A 1987 Steady state current flow in solid binary electrolyte cells *J. Electroanal. Chem.* **225** 1–17
[44] Evans J, Vincent C A and Bruce P G 1987 Electrochemical measurement of transference numbers in polymer electrolytes *Polymer* **28** 2324–8
[45] Aldalur I *et al* 2020 Nanofiber-reinforced polymer electrolytes toward room temperature solid-state lithium batteries *J. Power Sources* **448** 227424–31
[46] Nti F, Porcarelli L, Greene G W, Zhu H, Makhlooghiazad F, Mecerreyes D, Howlett P C, Forsyth M and Wang X 2020 The influence of interfacial interactions on the conductivity and phase behaviour of organic ionic plastic crystal/polymer nanoparticle composite electrolytes *J. Mater. Chem.* A **8** 5350–62
[47] Wang X *et al* 2016 Enhancement of ion dynamics in organic ionic plastic crystal/PVDF composite electrolytes prepared by co-electrospinning *J. Mater. Chem.* A **4** 9873–80
[48] Song S, Kotobuki M, Zheng F, Xu C, Savilov S V, Hu N, Lu L, Wang Y and Li W D Z 2017 A hybrid polymer/oxide/ionic-liquid solid electrolyte for Na-metal batteries *J. Mater. Chem.* A **5** 6424–31
[49] Vélez J F, Álvarez L V, Del Río C, Herradón B, Mann E and Morales E 2017 Imidazolium-based mono and dicationic ionic liquid sodium polymer gel electrolytes *Electrochim. Acta* **241** 517–25
[50] Gao Y, Chen G, Wang X, Yang H, Wang Z, Lin W, Xu H, Bai Y and Wu C 2020 PY13FSI-infiltrated SBA-15 as nonflammable and high ion-conductive ionogel electrolytes for quasi-solid-state sodium–ion batteries *ACS Appl. Mater. Interfaces* **12** 22981–91
[51] Hilder M, Howlett P C, Saurel D, Gonzalo E, Armand M, Rojo T, Macfarlane D R and Forsyth M 2017 Small quaternary alkyl phosphonium bis(fluorosulfonyl)imide ionic liquid electrolytes for sodium-ion batteries with P2- and O3-Na 2/3 [Fe 2/3 Mn 1/3]O 2 cathode material *J. Power Sources* **349** 45–51
[52] Pathirana T, Kerr R, Forsyth M and Howlett P C 2020 Electrochemical formation in super-concentrated phosphonium based ionic liquid electrolyte using symmetric Li-Metal coin cells *J. Electrochem. Soc.* **167** 120526–33
[53] Rakov D A, Chen F, Ferdousi S A, Li H, Pathirana T, Simonov A N, Howlett P C, Atkin R and Forsyth M 2020 Engineering high-energy-density sodium battery anodes for improved cycling with superconcentrated ionic-liquid electrolytes *Nat. Mater.* **19** 1096–101
[54] Xu L, Li J, Deng W, Li L, Zou G, Hou H, Huang L and Ji X 2021 Boosting the ionic conductivity of PEO electrolytes by waste eggshell-derived fillers for high-performance solid lithium/sodium batteries *Mater. Chem. Front.* **5** 1315–23
[55] Gao R, Tan R, Han L, Zhao Y, Wang Z, Yang L and Pan F 2017 Nanofiber networks of $Na_3V_2(PO_4)_3$ as a cathode material for high performance all-solid-state sodium-ion batteries *J. Mater. Chem.* A **5** 5273–7
[56] Jian Z *et al* 2013 Superior electrochemical performance and storage mechanism of $Na_3V_2(PO_4)_3$ cathode for room-temperature sodium–ion batteries *Adv. Energy Mater.* **3** 156–60